ARTICLE

Oligosaccharide/Silicon-Containing Block Copolymers with 5 nm Features for Lithographic Applications

Julia D. Cushen,[†,¶] Issei Otsuka,[§,¶] Christopher M. Bates,[‡] Sami Halila,[§] Sébastien Fort,[§] Cyrille Rochas,[§] Jeffrey A. Easley,[†] Erica L. Rausch,[†] Anthony Thio,[†] Redouane Borsali,[§,*] C. Grant Willson,[†,‡,*] and Christopher J. Ellison[†,*]

[†]Department of Chemical Engineering, The University of Texas at Austin, 1 University Station C0400, Austin, Texas 78712, United States, [‡]Department of Chemistry, The University of Texas at Austin, 1 University Station, A5300, Austin, Texas 78712, United States, and [§]Centre de Recherche sur les Macromolécules Végétales-CERMAV, CNRS UPR 5301-ICMG and Joseph Fourier University, BP53, 38041 Grenoble Cedex 9, France. [¶]These authors contributed equally to this work.

ABSTRACT Block copolymers demonstrate potential for use in next-generation lithography due to their ability to self-assemble into well-ordered periodic arrays on the 3–100 nm length scale. The successful lithographic application of block copolymers relies on three critical conditions being met: high Flory–Huggins interaction parameters (χ), which enable formation of <10 nm features, etch selectivity between blocks for facile pattern transfer, and thin film self-assembly control. The present paper describes the synthesis and self-assembly of block copolymers composed of naturally derived oligosaccharides coupled to a silicon-containing polystyrene derivative synthesized by activators regenerated by electron transfer atom transfer radical polymerization. The block copolymers have a large χ and a low degree of polymerization (N) enabling formation of 5 nm feature diameters, incorporate silicon in one block for oxygen reactive ion etch contrast, and exhibit bulk and thin film self-assembly of hexagonally packed cylinders facilitated by a combination of spin coating and solvent annealing techniques. As observed by small angle X-ray scattering and atomic force microscopy, these materials exhibit some of the smallest block copolymer features in the bulk and in thin films reported to date.

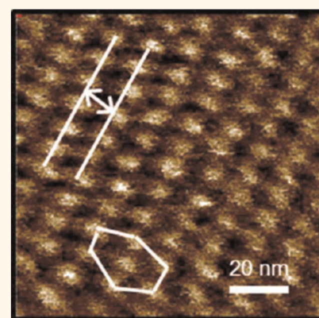

KEYWORDS: block copolymer · lithography · oligosaccharide · thin films · nanopatterning · poly(trimethylsilyl styrene)

The current 193 nm optical immersion lithography process has reached resolution limits at approximately 36 nm as described by Rayleigh's equation.[1] Alternative patterning technologies must be developed to enable manufacturing of next-generation integrated circuits, flash memory and hard disk drives. Nanoimprint technology is an attractive choice for replicating sub-36 nm features, and has demonstrated successful pattern transfer down to <3 nm.[2] However, economical creation of an imprint template remains a considerable challenge. Electron beam lithography is considered a prohibitively expensive alternative. For example, creating a bit-patterned magnetic storage media template with a 1 Tbit/in^2 dot array by electron beam lithography is estimated to require more than a month of continuous writing time at a cost exceeding 1 million dollars.[3] Block copolymers present a promising route for fabricating nanoscale patterns due to their ability to self-assemble into well-ordered periodic arrays with features well below 36 nm.[4–6] These self-assembled materials can be converted into lithographic templates upon removal of one block using processing steps that are compatible with current semiconductor fabrication such as spin coating, annealing, and etching.[7,8]

While a wide variety of block copolymer systems have been considered for use in nanoimprint template formation, three requirements for a successful material emerge; one block that can be easily removed (sacrificial), a strong driving force for microphase separation, and thin film self-assembly control. Template formation requires the selective removal of one block and subsequent pattern transfer into a substrate. However, most block copolymer systems, such as poly(styrene-*b*-methyl methacrylate),[9] have poor reactive ion etch selectivity between the blocks which limits patterns to low aspect-ratio features.[10] Furthermore, wet etching techniques are generally limited to relatively low aspect ratio features due to feature collapse.[11] Producing features with higher aspect ratios can be achieved with organic block copolymers, but this typically requires additional processing steps to selectively remove one

* Address correspondence to borsali@cermav.cnrs.fr, willson@che.utexas.edu, ellison@che.utexas.edu.

Received for review January 31, 2012 and accepted March 28, 2012.

Published online March 28, 2012
10.1021/nn300459r

© 2012 American Chemical Society

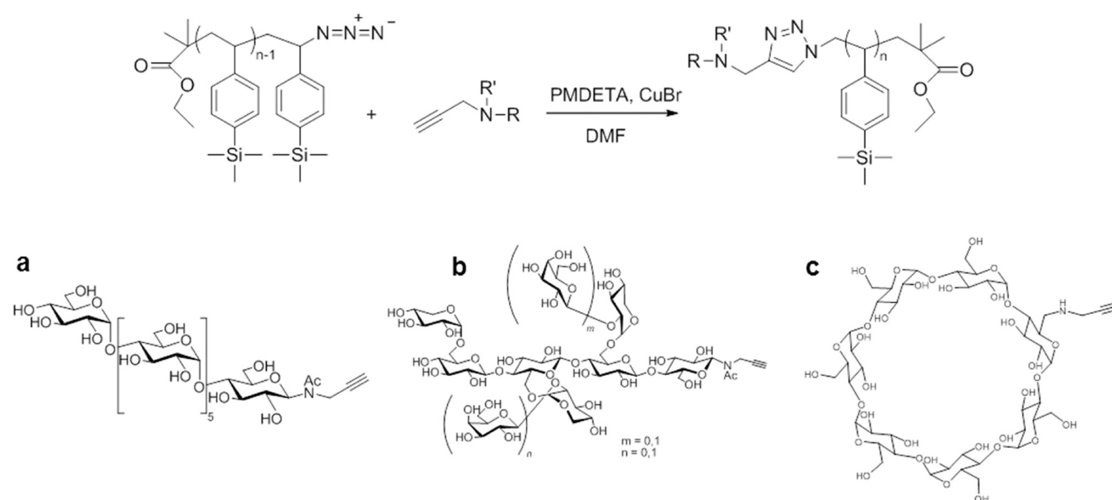

Scheme 1. Azide−alkyne cycloaddition of the oligosaccharide/silicon-containing block copolymers introduced in this study were (a) R = MH, R′ = Ac, (b) R = XGO, R′ = Ac, and (c) R = βCyD, R′ = H.

block and then transfer the pattern into a metal or semiconductor substrate.[8,12,13] Previous research has shown that incorporating a sufficient amount of silicon[14] or metal into one block creates an inorganic oxide etch mask when exposed to oxygen plasma. Materials such as poly(lactide-*b*-dimethylsiloxane-*b*-lactide) (PLA-*b*-PDMS-*b*-PLA),[15] poly(styrene-*b*-dimethylsiloxane) (PS-*b*-PDMS),[16] poly(styrene-*b*-ferrocenylsilane) (PS-*b*-PFS),[17] and polyhedral oligomeric silsesquioxane-containing polymers (PS-*b*-PMAPOSS)[18] demonstrate high etch contrast due to their inorganic components. With these polymers, the organic block can be completely removed in one etching step to create a nanoscale template.

The Flory−Huggins interaction parameter, χ, quantifies the thermodynamic driving force for microphase separation, which occurs when the product of the degree of polymerization (N) and the interaction parameter (χ), χN, is larger than a critical value (10.5 for symmetric diblocks).[6] Furthermore, the domain periodicity of microphase separation (d) scales as $d \sim aN^{2/3}\chi^{1/6}$ in the strong-segregation limit.[6] Since d is more strongly a function of N than χ, reducing N is the most favorable approach to decrease d, subject to the constraint that χN must be larger than a critical value for producing self-assembled structures. Thus, it is crucial to pursue block copolymers that have small N and high χ values to minimize self-assembled feature sizes while simultaneously maximizing feature densities for next-generation lithography. To this end, natural-*b*-synthetic "hybrid" block copolymer systems composed of an abundant, naturally derived poly- or oligo-saccharide block[19−22] are attractive because these block copolymers have been reported to self-assemble into well-ordered periodic arrays with roughly 10 nm domain spacing when polystyrene is the adjoining block. These exceedingly small features were achieved due to the very high incompatibility between the oligosaccharide block and the polystyrene block originating from their hydrophobicity/hydrophilicity imbalance which is further enhanced sterically by the rodlike nature of the oligosaccharide blocks, as compared to coil−coil or flexible−flexible block copolymer systems. In addition to nanopatterning, naturally derived poly- or oligosaccharide blocks have potential use in biomedical applications[23,24] due to their biocompatibility.

In this work, new diblock copolymers composed of poly(*para*-trimethylsilylstyrene) (PTMSS) tethered to oligosaccharides were synthesized through azide−alkyne "click" chemistry. The oligosaccharides are naturally derived materials that can be strategically modified with a terminal functional group, allowing them to be coupled to other polymers to form block copolymers. In the block copolymers described here, the hydrophobic silicon-containing block provides the etch resistance desirable for template patterning and chemical incompatibility with the hydrophilic oligosaccharide block, which results in large χ.

Finally, block copolymer self-assembly control must be achieved in thin films to maximize the utility of the self-assembled pattern. Self-assembly can be accomplished using thermal[25] and solvent annealing[26,27] techniques. Both are applied herein to control the bulk and thin film self-assembly of oligosaccharide/silicon-containing block copolymers. Their self-assembly results in cylinders with approximately 5 nm diameters, which the authors believe are some of the smallest block copolymer features reported to date.

RESULTS AND DISCUSSION

PTMSS was synthesized by activators regenerated by electron transfer atom transfer radical polymerization (ARGET ATRP),[28] a relatively new controlled radical polymerization method. The oligosaccharides were functionalized with a single alkyne group, and the two blocks were coupled by azide−alkyne cycloaddition as shown in Scheme 1. Ethynyl-functionalized

oligosaccharides, *N*-maltoheptaosyl-3-acetamido-1-propyne (ethynyl-MH), *N*-xyloglucooligosaccharide-3-acetamido-1-propyne (ethynyl-XGO), and mono-6^A-*N*-propargylamino-6^A-deoxy-β-cyclodextrin (ethynyl-βCyD), were coupled to azide-terminated PTMSS polymers with molecular weights of 4600 g/mol PDI = 1.09 and 2500 g/mol PDI = 1.30, denoted $PTMSS_{26}$ and $PTMSS_{15}$, respectively. The subscripts 26 and 15 denote the degree of polymerization of the PTMSS block. Material synthesis and characterization data can be found in the Supporting Information.

Small angle X-ray scattering (SAXS) studies were performed on bulk samples after solvent annealing in order to examine the morphologies and feature dimensions of the phase-separated materials. The oligosaccharide block has a relatively low thermal degradation temperature, and SAXS on bulk samples that were thermally annealed below the thermal degradation temperature of the oligosaccharide showed patterns consistent with a poorly ordered spherical structure. This is likely due to the fact that the glass transition temperature of the oligosaccharide block is above its degradation temperature and the polymer cannot gain sufficient mobility in the glassy state to reach a well-ordered conformation. Degradation and glass transition data from thermal gravimetric analysis and differential scanning calorimetry are provided in the Supporting Information.

Solvent vapor can be used in addition to or in place of thermal annealing to reach well-ordered structures since an appropriate solvent system can give the polymer chains mobility to self-assemble while at the same time removing defects.[26,27] Changes in the relative volume fractions and effective χ can occur during the solvent annealing process depending on the swelling ratio of each solvent in each block. These changes can induce morphological transitions in some cases. The solvent annealed self-assembled state can then be kinetically trapped upon removal of the solvent, yielding a nonequilibrium morphology and/or orientation. Solvent annealing the silicon-containing oligosaccharide bulk samples at room temperature in a well-sealed glass vial using the vapor produced from a 50:50 by volume THF/water liquid mixture led to well-ordered morphologies as evidenced by the evolution of bulk SAXS patterns. A THF/water mixture was chosen as the solvent system for these experiments because the PTMSS block is soluble in THF but has low solubility in water, and the oligosaccharide block is soluble in water but has low solubility in THF. This approach imparts mobility to both blocks of the copolymer that is necessary to enable rearrangement and enhanced ordering of the self-assembled structure. Solvent annealing experiments performed in only a hydrophilic solvent (water) or only a hydrophobic solvent (benzene) resulted in no improvement in the order of the system.

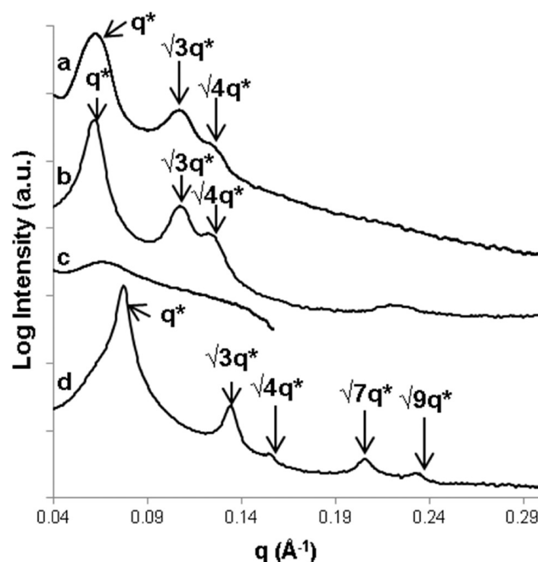

Figure 1. SAXS profiles after solvent annealing for (a) MH-*b*-$PTMSS_{26}$, (b) XGO-*b*-$PTMSS_{26}$, (c) βCyD-*b*-$PTMSS_{26}$, and (d) MH-*b*-$PTMSS_{15}$. Profiles are shifted vertically for clarity.

As shown in the SAXS profiles a and b in Figure 1, hexagonally packed cylindrical morphologies were observed in solvent annealed MH-*b*-$PTMSS_{26}$ and XGO-*b*-$PTMSS_{26}$ bulk samples as indicated by 1, $\sqrt{3}$, and $\sqrt{4}$ peak scattering ratios, q/q^*, where q^* is the position of the primary scattering peak. Given that the major component is PTMSS, it is likely that PTMSS is the continuous (or matrix) domain and the oligosaccharide is the cylinder domain. In contrast, the SAXS pattern of βCyD-*b*-$PTMSS_{26}$, profile c in Figure 1, appears disordered. Block copolymer domain spacings were calculated as $d = 2\pi/q^*$ and are 10.7 nm for MH-*b*-$PTMSS_{26}$ and 10.1 nm for XGO-*b*-$PTMSS_{26}$. Cylindrical feature diameters were calculated from the volume fractions of the blocks, determined from the molecular weights of the blocks and the densities of PTMSS[29] and amylose.[30] The calculated cylinder diameters are 5.2 nm for MH-*b*-$PTMSS_{26}$ and 5.1 nm for XGO-*b*-$PTMSS_{26}$. In MH-*b*-$PTMSS_{15}$, a bulk cylinder-forming morphology was also observed as indicated by the 1, $\sqrt{3}$, $\sqrt{4}$, and $\sqrt{7}$ peak scattering ratios in the SAXS pattern shown in profile d in Figure 1. The calculated domain spacing for this sample is 8.3 nm, which corresponds with feature diameters of 5.5 nm. Since the MH domain is unchanged, the cylinder diameter is roughly the same but the domain spacing, as defined by the primary scattering peak, is smaller.

It is important to note that 3 nm features have previously been achieved for a poly(styrene-*b*-ethylene oxide) block copolymer system with PS and PEO molecular weights of 5 and 2 kg/mol, respectively, under very specific conditions on a sawtooth-patterned substrate and in the presence of lithium tetrachloroaurate ($LiAuCl_4$).[31] $LiAuCl_4$ was used to favor microphase separation as well as to prevent dewetting

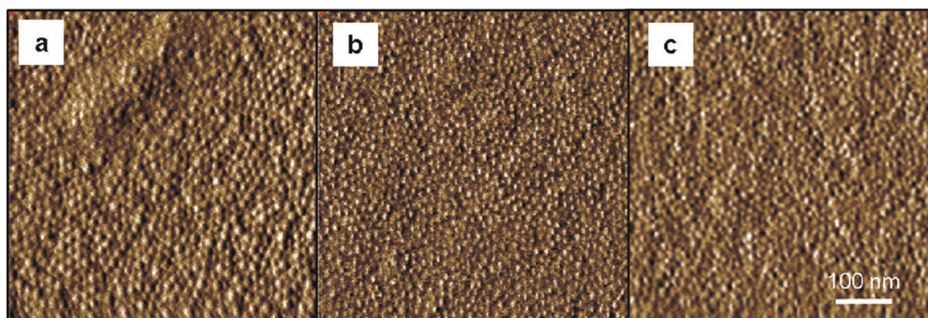

Figure 2. AFM phase images of as-cast MH-*b*-PTMSS$_{26}$ with thicknesses of (a) 6.8 nm, (b) 30.1 nm, and (c) 124 nm.

during solvent annealing of the low molar mass PS-*b*-PEO block copolymer. Unfortunaely, parts per billion or less of metal cannot be tolerated in conventional microelectronics fabrication processes. The present oligosaccharide-based block copolymer system does not require the presence of metals in any step of a lithography process and due to the high intrinsic incompatibility between the two blocks, 5 nm features were achieved without additives and on standard silicon substrates (see Figures 3, 4, and 5). For reference to bit-patterned media targets, if the ~5 nm oligosaccharide cylinders were arranged perpendicularly to the substrate surface in a thin film, areal feature densities greater than 8 Tbit/in^2 would be achieved, far exceeding the 1 Tbit/in^2 magnetic storage media industry target.

To explore the thin film self-assembly characteristics of the aforementioned ordered block copolymers, films were spin coated out of toluene. This solvent reproducibly produced smooth films without defects or film thickness variations. The as-cast, non-annealed films are shown in Figure 2 for a variety of film thicknesses of MH-*b*-PTMSS$_{26}$. These atomic force microscopy (AFM) phase images show poorly ordered circular features that we believe are trapped micelles. Toluene is a good solvent for the PTMSS block and a poor solvent for the oligosaccharide block, thus promoting formation of micelles in solution. The casting solutions were examined by dynamic light scattering (DLS), which confirmed the presence of micelles presumably consisting of a hydrophobic PTMSS corona around the hydrophilic oligosaccharide core. DLS results (Figure SI-7 in the Supporting Information) show peak particle diameters ranging from 12 to 22 nm for the different block copolymer samples. These spherical micelles were transferred from the casting solution to the substrate during spin coating, and we believe that they are kinetically trapped in the absence of any subsequent annealing steps. The circular features in Figure 2 appear to be locally hexagonally packed, but they are identical over a variety of film thicknesses ranging from a monolayer to 124 nm, which is a good indication that the as-cast samples are kinetically trapped spherical micelles deposited from the casting solution rather than some other self-assembled block copolymer structure. This explanation is also consistent with bulk scattering patterns collected from as precipitated bulk samples which indicated poorly ordered spheres.

Approximately 30 nm thick films of MH-*b*-PTMSS$_{26}$, XGO-*b*-PTMSS$_{26}$, βCyD-*b*-PTMSS$_{26}$, and MH-*b*-PTMSS$_{15}$ were examined before and after solvent vapor annealing in the presence of a 50/50 THF/water solution at room temperature, and then after subsequent thermal annealing. Figure 3 panels a and d show AFM phase images of MH-*b*-PTMSS$_{26}$ and XGO-*b*-PTMSS$_{26}$, respectively, as-cast before solvent or thermal annealing. The disordered circular features of as-cast XGO-*b*-PTMSS$_{26}$ are consistent with the micelles observed for the as-cast MH-*b*-PTMSS$_{26}$ shown in Figure 2 (micelles in the XGO-*b*-PTMSS$_{26}$ casting solution were also confirmed with DLS measurements). This result is in perfect agreement with the single broad shoulder observed in the SAXS profiles of non-annealed bulk MH-*b*-PTMSS$_{26}$ and XGO-*b*-PTMSS$_{26}$ systems as illustrated in Figure 3a,d.

AFM phase images of MH-*b*-PTMSS$_{26}$ and XGO-*b*-PTMSS$_{26}$ films exposed to 50/50 THF/water vapor for 24 h (Figure 3 panels b and e, respectively) exhibited regions of circular features (like those dominating Figure 3b), that could be interpreted as either ordered body-centered cubic spheres (BCC) or hexagonally packed cylinders oriented perpendicular to the substrate, together with regions of cylindrical domains oriented parallel to the substrate (like those dominating Figure 3e). Figure 3 panels c (MH-b-PTMSS$_{26}$) and f (XGO-b-PTMSS$_{26}$) show AFM images of solvent annealed samples, which were subsequently thermally annealed at 160 °C under vacuum for 15 min. SAXS patterns for Figure 3 images b, c, e, and 3f are consistent with hexagonally packed cylindrical morphology as illustrated by the scattering peaks located at $q/q^* = 1, \sqrt{3}$, and $\sqrt{7}$ for MH-*b*-PTMSS$_{26}$ and $q/q^* = 1, \sqrt{3}, \sqrt{4}, \sqrt{9}$, and $\sqrt{12}$ for XGO-*b*-PTMSS$_{26}$. Figure 3 shows that the domain spacing of the samples that were solvent annealed compared to those that were solvent annealed then heated differ by less than a few percent indicating that significant quantities of residual

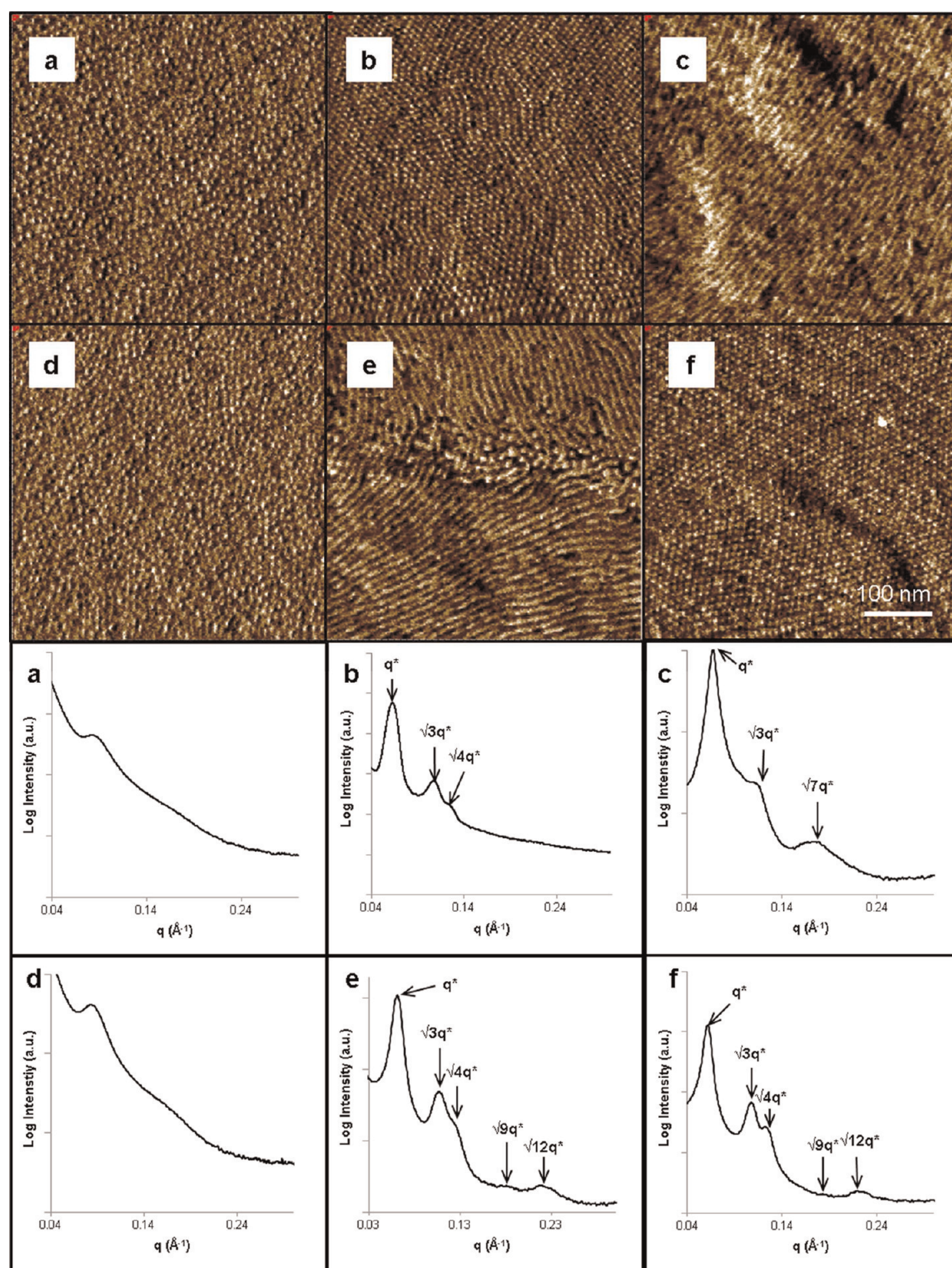

Figure 3. AFM thin film phase images and corresponding SAXS patterns of bulk samples of (a) as-cast MH-*b*-PTMSS$_{26}$, (b) MH-*b*-PTMSS$_{26}$ after solvent annealing, (c) MH-*b*-PTMSS$_{26}$ after solvent annealing then heating to 160 °C, (d) as-cast XGO-*b*-PTMSS$_{26}$, (e) XGO-*b*-PTMSS$_{26}$ after solvent annealing, and (f) XGO-*b*-PTMSS$_{26}$ after solvent annealing then heating to 160 °C, the highest temperature at which thermal annealing can be performed without degrading the oligosaccharide (see Supporting Information).

water or solvent may not be present after removing the sample from the solvent vapor. It has been reported that domain spacing and size can be kinetically trapped when one block of the block copolymer vitrifies during rapid solvent removal, a process which can happen in seconds after removal of a thin film from solvent vapor,[21] which could also be the case here.

While as presented in Figure 3 it appears that the MH-*b*-PTMSS$_{26}$ and XGO-*b*-PTMSS$_{26}$ each switch morphology and/or orientation in thin films as a result of

thermal annealing, this is not the case. In repeated experiments, areas with both circular structures and horizontal cylinder structures could be identified for almost all of the thermal and solvent annealing conditions tested. This observation led to the hypothesis that MH-*b*-PTMSS$_{26}$ and XGO-*b*-PTMSS$_{26}$, both with oligosaccharide volume fractions of approximately 15%, lie on or close to the BCC sphere/hexagonally packed cylinder phase boundary, which would promote coexistence of these mixed structures, even with their rod–coil block copolymer structure.[32] For such a condition, small perturbations in local film thickness, annealing time, drying, or local solvent vapor concentration during solvent annealing could induce mixed morphologies.

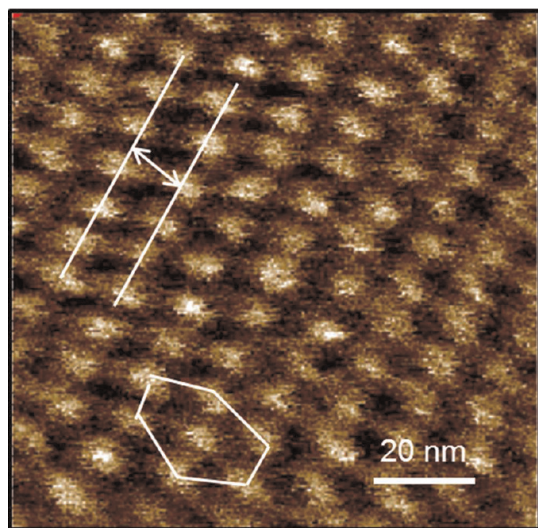

Figure 4. AFM phase image of MH-*b*-PTMSS$_{26}$ after solvent annealing. The row spacing between features shown in this image is 11.4 nm.

Unfortunately, it is not possible with a surface sensitive technique, such as AFM, to distinguish between BCC spheres and vertically oriented cylinders within a 30 nm thick film. Supporting evidence for mixed BCC spheres and cylinders can be identified in several regions of Figure 3e,c with what appears to be epitaxial transformations[33,34] between crystallographic planes of the BCC lattice and hexagonal packed cylinder lattice providing further evidence for close proximity to a phase boundary. None of the solvent annealed thin films show any evidence of a silicon wetting layer at the air interface. This is likely due to solvent absorption into each domain, which neutralizes the interfacial energy at the air–polymer interface making it nonpreferential for either block.[22] The nature of the substrate surface after solvent annealing remains unclear, but may be important for subsequent pattern transfer, which will be the subject of future investigations.

Figure 4 shows an enlarged region of the circular features in the 30 nm thick film that are evident in Figure 3b, highlighting the hexagonal packing and the very small feature size of what could be vertically aligned cylinders. From the AFM images presented

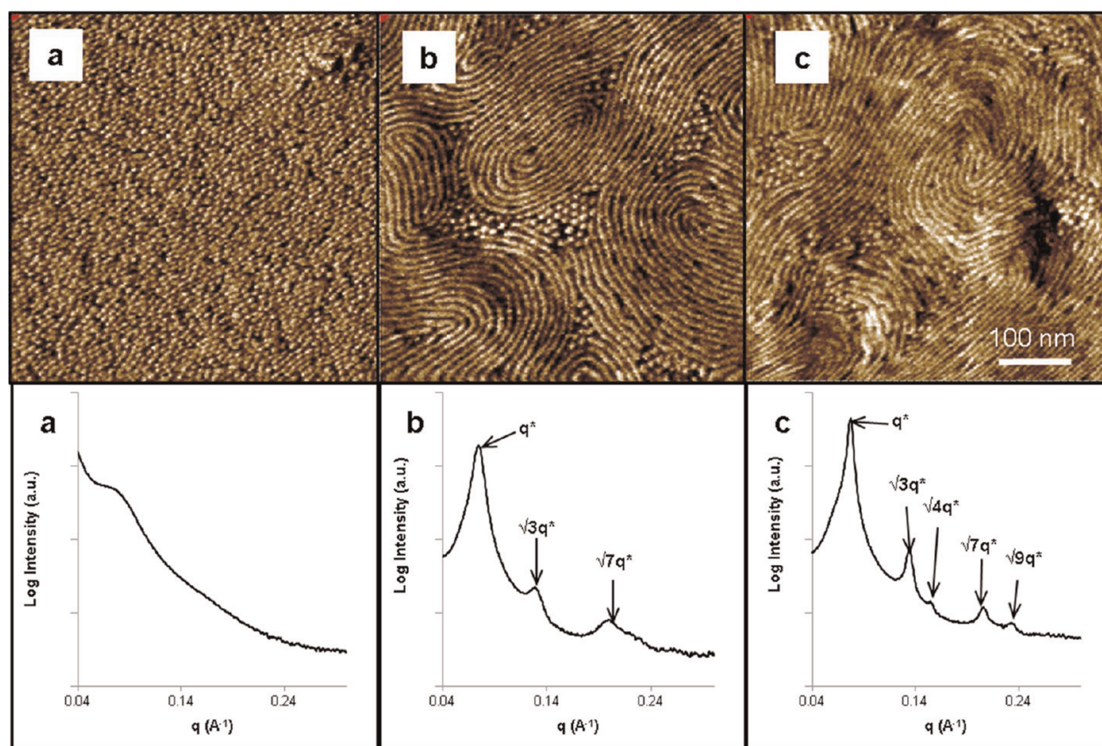

Figure 5. AFM phase images and corresponding SAXS patterns of (a) as-cast MH-*b*-PTMSS$_{15}$, (b) MH-*b*-PTMSS$_{15}$ after solvent annealing, (c) MH-*b*-PTMSS$_{15}$ after solvent annealing then heating.

herein, the size of the individual cylinder domains is measured to be approximately 8 nm. It should be noted that many factors, such as AFM tip size (the tip radius used here was reported by the manufacturer to be <10 nm), elastic moduli, instrument resolution, and domain boundary definition, contribute to the errors in the AFM measurement and can significantly impact the observed feature sizes. It is also possible that the domain size measured in this solvent annealed thin film is slightly larger than that calculated from the bulk SAXS measurement due to solvent uptake during solvent annealing and quenching of the domain structure after removal from the solvent vapor, a phenomenon seen by other researchers.[21]

In contrast to the results shown in Figure 3, the βCyD-*b*-$PTMSS_{26}$ as-cast films exhibited a poorly ordered micelle structure which reproducibly switched to a disordered state after solvent vapor annealing (see Supporting Information, Figure SI-6) consistent with bulk SAXS data in Figure 1c. There are several possible reasons why this block copolymer is disordered including the fact that βCyD may be a more rigid block that may distort the phase diagram boundaries through conformational asymmetry effects[35,36] or the fact that the effective N value (proportional to molecular weight) is sufficiently lower than that of MH or XGO.

A block copolymer that is further from the phase boundary between BCC and hexagonally packed cylinders was also synthesized and examined for comparison to those presented in Figure 3. This sample, MH-*b*-$PTMSS_{15}$, has an oligosaccharide volume fraction of 29.9% and was designed to be more deeply embedded in the cylinder part of the phase diagram. Consistent with the SAXS and AFM data presented in Figure 5, this polymer reproducibly exhibits a cylindrical morphology oriented parallel to the substrate with some isolated mixed circular features under all annealing conditions. This observation lends some credence to the hypothesis that the samples shown in Figure 3 are near the phase boundary.

TABLE 1. Thickness Measurements of Homopolymer Thin Films before and after a 30 s Oxygen Plasma Etch[a]

homopolymer film	initial thickness[b] (nm)	final thickness[b] (nm)	etch rate (nm/sec)
oligosaccharide	660 ± 20	300 ± 7	12.1 ± 0.6
PTMSS	135.6 ± 0.3	122.8 ± 0.5	0.43 ± 0.02

[a] The etch selectivity, defined here as the etch rate of the oligosaccharide divided by the etch rate of the PTMSS, is calculated to be 28.3. [b] The error is represented by the standard deviation, taken from three different measurements.

While the self-assembled features of these block copolymers are clearly much smaller than those that can be made by conventional photolithography, the block copolymer must have high etch contrast in order to be useful for creating high aspect ratio lithographic patterns in the fewest steps. Therefore, the etch rates of the oligosaccharide and PTMSS homopolymers were investigated to determine the etch selectivity between the blocks. A 15 wt % aqueous solution of a mixture of malto-oligosaccharides (degree of polymerization from 1 to 7) was spin-coated onto a mica substrate. The oligosaccharide mixture was chosen to suppress crystallization, which has been shown to decrease the etch rate of polymeric thin films relative to amorphous polymers.[37] A 4 wt % solution of PTMSS homopolymer was spin-coated onto a silicon wafer with approximately 4 nm native silicon dioxide. The homopolymer films were subjected to a 30 s oxygen etch (90 mTorr chamber pressure, 80 W RF power, 250 W ICP power, 75 sccm O_2 flow rate, 5 sccm Ar flow rate), and the film thicknesses were measured to determine etch rates. The results are summarized in Table 1.

The etch selectivity, defined as the oligosaccharide etch rate divided by the PTMSS etch rate, was determined to be 28.3, which represents a considerable improvement over fully petroleum-based block copolymers such as the ubiquitous poly(styrene-*b*-methyl methacrylate),[38] which has an etch selectivity of around 2 depending on the etch conditions.[38] Block copolymer thin films which were solvent annealed using the aforementioned conditions were subsequently exposed to an oxygen reactive ion etch. Because of the

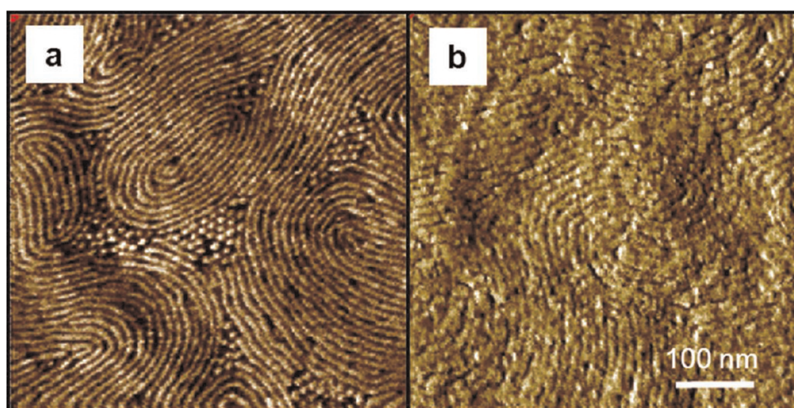

Figure 6. AFM phase images of MH-*b*-$PTMSS_{15}$ (a) after solvent annealing using 50/50 THF/water solvent vapor for 24 h and (b) after solvent annealing and then performing O_2 reactive ion etching.

extremely thin nature of the block copolymer film, the sub-10 nm feature sizes, and a plasma startup transient of our etch tool, the etch rates from Table 1 had to be significantly reduced. Etch conditions were adjusted to 20 mTorr chamber pressure, 10 W RF power, 50 W ICP power, 75 sccm O_2 flow rate, 75 sccm Ar flow rate, and 12 s etch time. Figure 6 shows AFM phase contrast inversion of the etched sample relative to the solvent annealed sample consistent with formation of an oxide layer over the PTMSS matrix domain and suggests at least partial removal of the oligosaccharide block.

CONCLUSIONS

In summary, the synthesis of new cylinder-forming oligosaccharide-*b*-PTMSS block copolymers by ARGET ATRP and azide–alkyne cycloaddition has been demonstrated. Bulk block copolymers exhibit cylinder-forming morphologies with approximately 5 nm diameter cylinders, as characterized by SAXS. Thin film self-assembly of these polymers has been realized through a combination of spin coating and solvent annealing on standard silicon wafer substrates. Such small features, mainly due to the strong incompatibility between the two blocks, enable areal feature densities for magnetic information storage devices approaching 8 Tbit/in^2, far exceeding the 1 Tbit/in^2 magnetic storage media industry target for bit-patterned media. Furthermore, reactive ion etch studies on homopolymer and block copolymer films have demonstrated the etch resistance of the silicon-containing block relative to the oligosaccharide, which will aid in using these materials for constructing nanoimprint templates.

METHODS

p-Trimethylsilylstyrene (TMSS) was synthesized by a Grignard reaction according to a literature procedure.[39] The monomer was polymerized by ARGET ATRP[28] and end-functionalized with an azide group.[40] Ethynyl-MH, ethynyl-XGO, and ethynyl-βCyD were synthesized as described elsewhere.[20,41,42] The ethynyl-oligosaccharides and PTMSSAz polymers were coupled by azide–alkyne cycloaddition as previously reported.[19] All polymers and their properties along with detailed synthesis protocols are reported in the supporting data.

Gel permeation chromatography (GPC) measurements were performed using a Viscotek VE 2001 triple-detector gel permeation chromatograph. THF was used as the eluent, with a flow rate of 1.0 mL min^{-1}. Samples were dissolved in THF (5 mg mL^{-1}) before analysis. All ^{1}H nuclear magnetic resonance (NMR) spectra were recorded on a Varian Unity Plus 400 MHz instrument using chloroform-d or dimethylformamide-d as the solvent. Chemical shifts are reported in ppm downfield from TMS using the residual protonated solvent as an internal standard ($CDCl_3$, ^{1}H 7.24 ppm or DMF-d, ^{1}H 2.91 ppm). Infrared spectroscopy (IR) data were recorded on a Nicolet 550 infrared spectrometer. The success of the azide–alkyne cycloaddition reaction was confirmed by IR, GPC, and NMR. Detailed polymer characterization data is reported in the Supporting Information. Thermogravimetric analysis (TGA) was conducted on a Mettler-Toledo TGA/DSC 1 thermogravimetric analyzer using a ramp rate of 10 °C per minute up to 1000 °C under nitrogen gas. TGA indicates that 160 °C is the highest temperature thermal annealing can be performed without degrading the oligosaccharide (see Supporting Information). Differential scanning calorimetry (DSC) experiments were performed on a Mettler Toledo DSC-1 under a nitrogen purge and at a heating rate of 20 °C per minute. Data are reported on the second heat.

The SAXS experiments were carried out at UT and at the European Synchrotron Radiation Facility (ESRF). At UT facilities, the SAXS measurements for Figure 1a,c and Figure 3b were collected using Cu Kα radiation (λ = 1.5418 Å) from a Molecular Metrology instrument using a high brilliance rotating copper anode source and a two-dimensional 120 mm gas filled multiwire detector. Vertical focus was achieved with a single crystal Ge mirror and horizontal focus and wavelength selection were achieved with an asymmetric cut Si(111) monochromator. The beam center was calibrated using silver behenate with the primary reflection peak at 1.076 nm^{-1}. These data were collected under vacuum at ambient temperature. Bulk samples were solvent annealed in a tightly capped 125 mL jar (Fisher, catalog no. 02-911-455) at room temperature for 24 h at atmospheric pressure. Within the jar was an uncapped 20 mL vial (Fisher, catalog no. 03-337-15) filled with a mixture of 2.5 g of THF and 2.5 g of water.

At ESRF facilities: SAXS experiments for Figure 1b, Figure 1d, Figure 3a, 3c–f, and Figure 4a–c were performed on the BM02 beamline of the ESRF (Grenoble, France). Bulk samples were put into glass capillaries of 1.5 mm diameter and then flame-sealed. The samples were disposed in sample holders equipped with an integrated heating system. The experiments were performed using 14 keV (λ = 0.089 nm) X-rays. Scattered intensities were recorded during 3–20 s exposures on a CCD detector placed about 78 cm behind the sample. These data were all collected at ambient pressure. ESRF SAXS data for samples designated as "solvent annealed" were collected at ambient temperature while ESRF SAXS data for samples designated as "solvent annealed then heated" were collected at 160 °C after several minutes of thermal annealing at that temperature. From analysis of all SAXS experiments that were performed on both instruments (at ESRF and UT), there is less than a few percent change in the domain spacing between samples that were "solvent annealed" compared to "solvent annealed then heated" indicating residual water or solvent significantly swelling domain spacing was not a major issue.

Thin films were prepared for AFM by spin coating 1 wt % polymer solutions in toluene at 2000 rpm for 60 s onto a silicon wafer with a native oxide layer. DLS measurements were performed on the spin-casting solutions using a Zetasizer nano ZS instrument. Films were spin coated on a Brewer CEE 100CB Spincoater. Film thicknesses were determined with a J.A. Woollam Co, Inc. VB 400 VASE Ellipsometer using wavelengths from 382 to 984 nm with a 65° angle of incidence. AFM data were collected at ambient temperature and pressure. Thin film samples designated as "solvent annealed" were solvent annealed for 24 h using the same setup as for the bulk SAXS samples and imaged immediately after solvent annealing without further treatment; samples designed as "solvent annealed then heated" were imaged after identical solvent annealing followed by thermal annealing at 160 °C under vacuum (~100 mTorr or less) for 15 min. Phase images are shown in this work and were obtained using an Agilent 5500 AFM in tapping mode. All AFM images were obtained using 300 series tapping mode AFM tips (reported tip radius <10 nm) from Ted Pella with a resonant frequency of 300 kHz and a force constant of 40 N/m.

Polymer solutions for etch studies were filtered with 0.20 μm PTFE filters prior to spin coating. Mica substrates (highest grade V1 mica discs) were purchased from Ted Pella. Prior to ellipsometric measurements, mica substrates were scratched on the back side of the substrate (where no thin film resided) with fine sandpaper to reduce reflections from the back surface. Oxygen plasma etching was performed with an Oxford Instruments Plasma Lab 80+ operating in inductively coupled plasma mode.

Conflict of Interest: The authors declare no competing financial interest.

Acknowledgment. The authors thank Nissan Chemical Company and CNRS for financial support. R. Borsali thanks the RTRA Nanosciences (Grant No. FCSN-2007-13P). C. Ellison also thanks the Welch Foundation (Grant No. F-1709) for partial financial support. This work was also supported by the National Science Foundation through a Graduate Research Fellowship to J. Cushen. AFM, SAXS, DLS, and oxygen plasma etching were performed using facilities at the Texas Materials Institute (TMI). The authors would also like to thank S. Swinnea and Y. Nishiyama for help with SAXS measurements. Mrs. P. Chaud and S. Pradeau are acknowledged for their help in the preparation of alkynyl oligosaccharides and S. Boullanger for the mass spectrometry analysis.

Supporting Information Available: Detailed description of block copolymer synthesis and characterization. (Table SI-1) Properties and compositions of polymers in this study; (Figure SI-1) NMR spectra showing transformation from bromine- to azide-terminated PTMSS; (Figure SI-2) GPC traces from the refractive index detector showing peak shifts to higher molecular weight polymer from $PTMSS_{26}$ to the block copolymers; (Figure SI-3) transmission IR spectra of PTMSSBr, PTMSSAz, and PTMSS-*b*-oligosaccharide after coupling; (Figure SI-4) DSC traces if PTMSS and oligosaccharides; (Figure SI-5) TGA data showing the degradation data for PTMSS and the oligosaccharides; (Figure SI-6) βCyD-*b*-$PTMSS_{26}$ as-cast and after solvent annealing; (Figure SI-7) dynamic light scattering on 0.5 wt % solutions in toluene of MH-$PTMSS_{26}$, XGO-*b*-$PTMSS_{26}$, βCyD-*b*-$PTMSS_{26}$, and MH-$PTMSS_{15}$. This material is available free of charge *via* the Internet at http://pubs.acs.org.

REFERENCES AND NOTES

1. Lin, B. J. Immersion Lithography and Its Impact on Semiconductor Manufacturing. *J. Microlithogr. Microfabr. Microsyst.* **2004**, *3*, 377–395.
2. Hua, F.; Sun, Y. G.; Gaur, A.; Meitl, M. A.; Bilhaut, L.; Rotkina, L.; Wang, J. F.; Geil, P.; Shim, M.; Rogers, J. A.; Shim, A. Polymer Imprint Lithography with Molecular-Scale Resolution. *Nano Lett.* **2004**, *4*, 2467–2471.
3. Ruiz, R.; Kang, H. M.; Detcheverry, F. A.; Dobisz, E.; Kercher, D. S.; Albrecht, T. R.; de Pablo, J. J.; Nealey, P. F. Density Multiplication and Improved Lithography by Directed Block Copolymer Assembly. *Science* **2008**, *321*, 936–939.
4. Kim, H.-C.; Park, S.-M.; Hinsberg, W. D. Block Copolymer Based Nanostructures: Materials, Processes, and Applications to Electronics. *Chem. Rev.* **2010**, *110*, 146–177.
5. Bates, F. S.; Fredrickson, G. H. Block Copolymers—Designer Soft Materials. *Phys. Today* **1999**, *52*, 32–38.
6. Bates, F. S.; Fredrickson, G. H. Block Copolymer Thermodynamics: Theory and Experiment. *Annu. Rev. Phys. Chem.* **1990**, *41*, 525–557.
7. Segalman, R. A. Patterning with Block Copolymer Thin Films. *Mater. Sci. Eng.: R* **2005**, *48*, 191–226.
8. Park, M.; Harrison, C.; Chaikin, P. M.; Register, R. A.; Adamson, D. H. Block Copolymer Lithography: Periodic Arrays of $\sim 10^{11}$ Holes in 1 Square Centimeter. *Science* **1997**, *276*, 1401–1404.
9. Thurn-Albrecht, T.; Schotter, J.; Kastle, C. A.; Emley, N.; Shibauchi, T.; Krusin-Elbaum, L.; Guarini, K.; Black, C. T.; Tuominen, M. T.; Russell, T. P. Ultrahigh-Density Nanowire Arrays Grown in Self-Assembled Diblock Copolymer Templates. *Science* **2000**, *290*, 2126–2129.
10. Asakawa, K.; Hiraoka, T.; Hieda, H.; Sakurai, M.; Kamata, Y. Nano-patterning for Patterned Media Using Block-Copolymer. *J. Photopolym. Sci. Technol.* **2002**, *15*, 465–470.
11. Delcambre, S. P.; Riggleman, R. A.; de Pablo, J. J.; Nealey, P. F. Mechanical Properties of Antiplasticized Polymer Nanostructures. *Soft Matter* **2010**, *6*, 2475–2483.
12. Zschech, D.; Kim, D. H.; Milenin, A. P.; Scholz, R.; Hillebrand, R.; Hawker, C. J.; Russell, T. P.; Steinhart, M.; Gosele, U. Ordered Arrays of ⟨100⟩-Oriented Silicon Nanorods by CMOS-Compatible Block Copolymer Lithography. *Nano Lett.* **2007**, *7*, 1516–1520.
13. Jeong, S. J.; Xia, G. D.; Kim, B. H.; Shin, D. O.; Kwon, S. H.; Kang, S. W.; Kim, S. O. Universal Block Copolymer Lithography for Metals, Semiconductors, Ceramics, and Polymers. *Adv. Mater.* **2008**, *20*, 1898–1904.
14. Colburn, M.; Grot, A.; Amistoso, M.; Choi, B. J.; Bailey, T.; Ekerdt, J.; Sreenivasan, S. V.; Hollenhorst, S.; Willson, C. G., Step and Flash Imprint Lithography for Sub-100nm Patterning. In *Emerging Lithographic Technologies IV*; Dobisz, E. A., Ed.; SPIE-Int Soc Optical Engineering: Bellingham, WA, 2000; Vol. 3997, pp 453−457.
15. Rodwogin, M. D.; Spanjers, C. S.; Leighton, C.; Hillmyer, M. A. Polylactide-Poly(dimethylsiloxane)-Polylactide Triblock Copolymers as Multifunctional Materials for Nanolithographic Applications. *ACS Nano* **2010**, *4*, 725–732.
16. Jung, Y. S.; Ross, C. A. Orientation-Controlled Self-Assembled Nanolithography Using a Polystyrene-Polydimethylsiloxane Block Copolymer. *Nano Lett.* **2007**, *7*, 2046–2050.
17. Chuang, V. P.; Ross, C. A.; Gwyther, J.; Manners, I. Self-Assembled Nanoscale Ring Arrays from a Polystyrene-*b*-Polyferrocenylsilane-*b*-Poly(2-Vinylpyridine) Triblock Terpolymer Thin Film. *Adv. Mater.* **2009**, *21*, 3789–3793.
18. Hirai, T.; Leolukman, M.; Liu, C. C.; Han, E.; Kim, Y. J.; Ishida, Y.; Hayakawa, T.; Kakimoto, M.-a.; Nealey, P. F.; Gopalan, P. One-Step Direct-Patterning Template Utilizing Self-Assembly of POSS-Containing Block Copolymers. *Adv. Mater.* **2009**, *21*, 4334–4338.
19. Aissou, K.; Otsuka, I.; Rochas, C.; Fort, S.; Halila, S.; Borsali, R. Nano-organization of Amylose-*b*-Polystyrene Block Copolymer Films Doped with Bipyridine. *Langmuir* **2011**, *27*, 4098–4103.
20. Otsuka, I.; Fuchise, K.; Halila, S.; Fort, S.; Aissou, K.; Pignot-Paintrand, I.; Chen, Y.; Narumi, A.; Kakuchi, T.; Borsali, R. Thermoresponsive Vesicular Morphologies Obtained by Self-Assemblies of Hybrid Oligosaccharide-Block-Poly (*N*-isopropylacrylamide) Copolymer Systems. *Langmuir* **2010**, *26*, 2325–2332.
21. Jeong, J. W.; Park, W. I.; Kim, M.-J.; Ross, C. A.; Jung, Y. S. Highly Tunable Self-Assembled Nanostructures from a Poly(2-vinylpyridine-*b*-dimethylsiloxane) Block Copolymer. *Nano Lett.* **2011**, *11*, 4095–4101.
22. Albert, J. N. L.; Epps, T. H., III Self-Assembly of Block Copolymer Thin Films. *Mater. Today* **2010**, *13*, 24–33.
23. Staats, H. F.; Leong, K. W. Polymer Hydrogels: Chaperoning Vaccines. *Nat. Mater.* **2010**, *9*, 537–538.
24. Wang, D.-A.; Varghese, S.; Sharma, B.; Strehin, I.; Fermanian, S.; Gorham, J.; Fairbrother, D. H.; Cascio, B.; Elisseeff, J. H. Multifunctional Chondroitin Sulphate for Cartilage Tissue−Biomaterial Integration. *Nat. Mater.* **2007**, *6*, 385–392.
25. Ji, S. X.; Liu, C. C.; Liao, W.; Fenske, A. L.; Craig, G. S. W.; Nealey, P. F. Domain Orientation and Grain Coarsening in Cylinder-Forming Poly(styrene-*b*-methyl methacrylate) Films. *Macromolecules* **2011**, *44*, 4291–4300.
26. Kim, G.; Libera, M. Morphological Development in Solvent-Cast Polystyrene−Polybutadiene−Polystyrene (SBS) Triblock Copolymer Thin Films. *Macromolecules* **1998**, *31*, 2569–2577.
27. Cavicchi, K. A.; Berthiaume, K. J.; Russell, T. P. Solvent Annealing Thin Films of Poly(isoprene-*b*-lactide). *Polymer* **2005**, *46*, 11635–11639.
28. Jakubowski, W.; Kirci-Denizli, B.; Gil, R. R.; Matyjaszewski, K. Polystyrene with Improved Chain-End Functionality and Higher Molecular Weight by ARGET ATRP. *Macromol. Chem. Phys.* **2008**, *209*, 32–39.
29. Harada, M.; Suzuki, T.; Ohya, M.; Kawaguchi, D.; Takano, A.; Matsushita, Y. Novel Miscible Polymer Blend of Poly-(4-trimethylsilylstyrene) and Polyisoprene. *Macromolecules* **2005**, *38*, 1868–1873.
30. Takahashi, Y.; Kumano, T.; Nishikawa, S. Crystal Structure of β-Amylose. *Macromolecules* **2004**, *37*, 6827–6832.
31. Park, S.; Lee, D. H.; Xu, J.; Kim, B.; Hong, S. W.; Jeong, U.; Xu, T.; Russell, T. P. Macroscopic 10-Terabit-per-Square- Inch Arrays from Block Copolymers with Lateral Order. *Science* **2009**, *323*, 1030–1033.

32. Sary, N.; Rubatat, L.; Brochon, C.; Hadziioannou, G.; Ruokolainen, J.; Mezzenga, R. Self-Assembly of Poly(diethylhexyloxy-*p*-phenylenevinylene)-*b*-Poly(4-vinylpyridine) Rod-Coil Block Copolymer Systems. *Macromolecules* **2007**, *40*, 6990–6997.
33. Kimishima, K.; Koga, T.; Hashimoto, T. Order−Order Phase Transition between Spherical and Cylindrical Microdomain Structures of Block Copolymer. I. Mechanism of the Transition. *Macromolecules* **2000**, *33*, 968–977.
34. Matsen, M. W. Cylinder−Sphere Epitaxial Transitions in Block Copolymer Melts. *J. Chem. Phys.* **2001**, *114*, 8165–8173.
35. Bates, F. S.; Schulz, M. F.; Khandpur, A. K.; Forster, S.; Rosedale, J. H.; Almdal, K.; Mortensen, K. Fluctuations, Conformational Asymmetry and Block Copolymer Phase Behaviour. *Faraday Discuss.* **1994**, *98*, 7–18.
36. Matsen, M. W.; Bates, F. S. Conformationally Asymmetric Block Copolymers. *J. Polym. Sci., Part B:* **1997**, *35*, 945–952.
37. Wohlfart, E.; Fernandez-Blazquez, J. P.; Knoche, E.; Bello, A.; Perez, E.; Arzt, E.; del Campo, A. Nanofibrillar Patterns by Plasma Etching: The Influence of Polymer Crystallinity and Orientation in Surface Morphology. *Macromolecules* **2010**, *43*, 9908–9917.
38. Farrell, R. A.; Petkov, N.; Shaw, M. T.; Djara, V.; Holmes, J. D.; Morris, M. A. Monitoring PMMA Elimination by Reactive Ion Etching from a Lamellar PS-b-PMMA Thin Film by *ex Situ* TEM Methods. *Macromolecules* **2010**, *43*, 8651–8655.
39. Harada, M.; Suzuki, T.; Ohya, M.; Takano, A.; Matsushita, Y. Preparation of Partially Deuterium-Labeled Poly(4-trimethylsilylstyrene)s and Unperturbed Dimensions in Bulk. *Polym. J.* **2004**, *36*, 538–541.
40. Coessens, V.; Matyjaszewski, K. End Group Transformation of Polymers Prepared by ATRP, Substitution to Azides. *J. Macromol. Sci., Part A: Pure Appl. Chem.* **1999**, *A36*, 667–679.
41. Halila, S.; Manguian, M.; Fort, S.; Cottaz, S.; Hamaide, T.; Fleury, E.; Driguez, H. Syntheses of Well-Defined Glycopolyorganosiloxanes by "Click" Chemistry and Their Surfactant Properties. *Macromol. Chem. Phys.* **2008**, *209*, 1282–1290.
42. Guo, Z.; Jin, Y.; Liang, T.; Liu, Y.; Xu, Q.; Liang, X.; Lei, A. Synthesis, Chromatographic Evaluation and Hydrophilic Interaction/Reversed-Phase Mixed-Mode Behavior of a "Click [Beta]-Cyclodextrin" Stationary Phase. *J. Chromatogr. A* **2009**, *1216*, 257–263.